

Propulsive performance of a windsurf-inspired pitching foil

Gauthier Bertrand¹, Tristan Aurégan¹, Benjamin Thiria¹, Ramiro Godoy-Diana¹, and Marc Fermigier¹

¹*Laboratoire de Physique et Mécanique des Milieux Hétérogènes (PMMH), CNRS UMR 7636, ESPCI Paris—Université PSL, Sorbonne Université, Université Paris Cité, F-75005 Paris, France*

We study experimentally a symmetrical rigid foil performing pitching oscillations around a mean incidence angle (α_m) with respect to an incoming flow in a hydrodynamic channel at a constant velocity where the Reynolds number according to the chord of the foil is, $Re_c = \rho U_\infty c / \mu = 14400$. The problem is inspired from the pumping maneuver used by athletes on the new hydrofoil-based windsurf boards. The goal of the study is to quantify the forces on this configuration by varying the pitching kinematics characterized by the Strouhal number ($St_A = fA/U_\infty$), from 0 to 0.27, and the mean incidence angle α_m , from 0 to 30°, of the foil. The force measurements show a high lift production and the delay of the stall angle according to St_A which can be linked to previous studies about the generation of vortices at the trailing edge. A general trend of decrease is observed for the drag force coefficient in pitching compare to the static case. For the highest Strouhal numbers tested, drag coefficient can become negative (thrust) in a range of α_m up to 15° in specific case. We present the various impacts of the amplitude of beating and the frequency of pitching on the aerodynamic forces for small mean incidence angle and high mean incidence angle (above the static stall angle). By using a sport-mimetic approach, we transform the measured lift & drag forces into a propulsive and drifting force. Doing so allows us to investigate race strategies. We investigate the generation of propulsion in upwind conditions.

I. INTRODUCTION

The competitive practice of sailing and windsurfing has seen a recent revolution with the introduction of new appendices of hydrofoils that generate lift and keep the board or the boat out of the water for a sufficiently high sailing speed [1]. This allows to increase the speed significantly because the wave drag and the hydrodynamic drag are almost suppressed. These innovations include the new iQFOil class introduced for the 2024 Olympic Games.

In order to improve the performance of sailboats and optimise their racing strategy, it is important to characterise their aerodynamic and hydrodynamic response [2]. Numerous studies on sails have been carried out experimentally in wind tunnels or under real conditions [3–6]. In particular, several works have studied the unsteady effects linked to environmental factors (sea state, wind) or to the dynamic actions of the crew, which can influence the performance of the sails [7–11]. In a laboratory context, a pitching or heaving foil is a reasonably good model to study the generation of unsteady forces which affect the sail propulsion. Young et al. [12] studied experimentally an unsteady propulsion method called sail flicking with a symmetrical rigid foil. With this sailing-mimetic approach, they found a high-lift mode in the optimal heaving direction where the foil can produce up to six times the lift in static mode.

During race starts or in low wind conditions, particularly after maneuvers like tacking which consist in turning the bow toward and through the wind to go upwind (Figure 1.a), windsurf athletes employ a technique called pumping to initiate or maintain foiling. This involves rhythmically adjusting the sail’s angle relative to the wind, providing intermittent propulsion to keep the board airborne. A theoretical and numerical study was conducted to examine the performance of a pumping sail according to complex parameters for windsurfing as a symmetrical foil (NACA 0012) by Zhou et al. [13]. They analysed the efficiency and the unsteady drive force, which is the projected aerodynamic force in the boat traveling direction (Figure 1.b), according to flapping parameters and sailing kinematics parameters. In these studies, the unsteady propulsion methods are effective in upwind condition (Figure 1.a). When windsurf athletes perform the pumping motion, the resulting sail kinematics is three-dimensional, but a reasonable leading-order model can be obtained by limiting the motion to a rotation around the vertical axis. In the present work, we will use such a simplified model: a pitching foil.

The dynamics of a foil subjected to oscillation has been a matter of interest for several decades for avoiding or reducing undesirable effects such as wing flutter and gust effect, but also to target benefits of the unsteady propulsion [14]. The study of a flapping foil has major implications in various fields such as propellers and turbomachinery and wind turbines [15], but also in animal locomotion [16, 17]. In the case of sailing or windsurfing, even without pumping movement, the sail propels the boat, so it is a different problem the self-propulsion case of animal locomotion.

A significant amount of experimental works have been conducted to study the physical parameters involved in flapping motion, leading to a better understanding of the generation of unsteady thrust force using flow visualisation techniques and force and moment sensors (Platzer et al. [18]). The optimal values of thrust force or propulsive efficiency are correlated with inverted Bénard-von Kármán type vortex wakes at the trailing edge [19, 20]. Flow visualisation has enabled the identification of different vortex wake structures as a function of flapping amplitude and frequency [21, 22]. Floryan et al. [23] propose scaling laws verified by experiments of thrust, power coefficients and efficiency for a heaving and pitching foil, which summarizes the influence of physical parameters. This is done for a foil with a mean incidence angle of zero, preventing the use of the scaling law of thrust for the windsurf case. The goal of this paper is to investigate the influence of a wide range of incidence angles in the performance

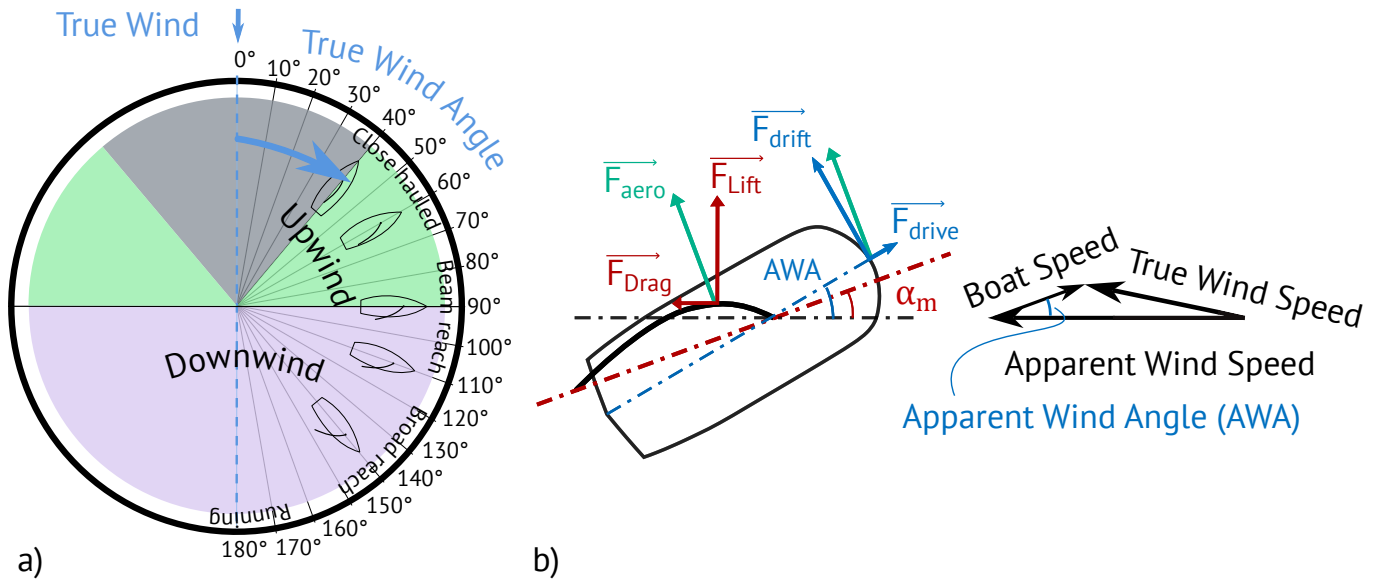


FIG. 1: a) The different points of sail of a sailing boat. The angle between the real wind positioned vertically and the longitudinal axis of the boat (reference line) is the True Wind Angle (TWA). b) Diagram of the dynamics of a sailboat associated with the sailing speed triangle, taking into account the forces applied to the sail and foil. Decomposition of the aerodynamic force (green) in the frame of reference of the boat (blue) and the flow (red).

of a pitching foil.

Few experimental studies, such as those by Ohmi et al. [24, 25], have examined the influence of a mean incidence angle around which the foil oscillates. They conducted a study on the vortex wake behind a symmetrical NACA 0012 profile, for two mean incidence angles (15° & 30°) and for each of these mean positions, two amplitudes ($\pm 7^\circ$ & $\pm 15^\circ$) and several frequencies. This provides them with a wide range of Strouhal number ($St_A = fA/U_\infty$, f is the pitching frequency and A the beating amplitude) values from 0.048 to 1.03. This range of St_A encompasses that of our study (Table I). They conclude that the mean incidence angle can contribute more than the position of the pivot or the shape of the foil to the generation of different wakes. Also, they determined that the vortex wake is St_A dependent. This study is done without measuring the associated unsteady forces. However, for a motion composed of pitching and heaving other studies discuss the useful effect of adding a non-zero mean incidence angle for maneuvers allowing a strong increase of unsteady side (lift) force coefficient thanks to the effects of the Leading-Edge Vortex (LEV) [26]. The generation of LEV affects the propulsion force and efficiency but not the time-averaged lift force [27]. In addition, the effect of large amplitudes and Reynolds number effect on the generation of forces and wakes for a pure pitching motion have been studied in particular by Zheng et al. [28] and Mackowski & Williamson [29], who also highlight the dynamic stall delay. We understand that the effect at the trailing edge is important in the generation of unsteady forces. LEVs appear when a foil is pitching or heaving with large amplitude or when it has a mean incidence angle large enough for this dynamic effect. In certain conditions of foil motion, it is possible to increase the lift force and delay its dynamic stall [14]. In windsurf, athletes navigate with various condition of wind, from small to high incidence angles of the sail where LEV might be produced, increasing the lift force.

We present an experimental study with a symmetrical shape of sail where a pitching movement is applied for various frequencies and amplitudes in a wide range of mean incidence angles to mimic the behavior of a sail under real sailing conditions, especially upwind conditions (Figure 1).

We define the True Wind Angle (TWA) as in Figure 1.a to define how the boat is moving according to the True Wind direction, consistent with nautical studies. The points of sail of the boat are also described in Figure 1.a. A sketch of the balance of forces applied on the sail according to the direction of the wind is shown in Figure 1.b.

The boat has a driving direction given by the Boat Speed (BS). The Apparent Wind Speed (AWS) is the composition of the BS and the True Wind Speed (TWS) and represents the wind perceived by the boat. The Apparent Wind Angle (AWA) is the angle between BS and AWS. The sail produces aerodynamic forces depending on the angle of incidence (α_m). AWA and α_m are independent, but both of them influence the drive and the drift forces and so the performance of the boat (Figure 1.b).

In this study, we will initially examine the impact of pumping amplitude and frequency, as well as the influence of mean incidence, by comparing measurements of lift and drag forces on a symmetrical profile. Subsequently, the forces within the boat's frame of reference (drive and drift forces) are studied in order to identify strategies for implementing pumping in accordance with the prevailing sailing conditions.

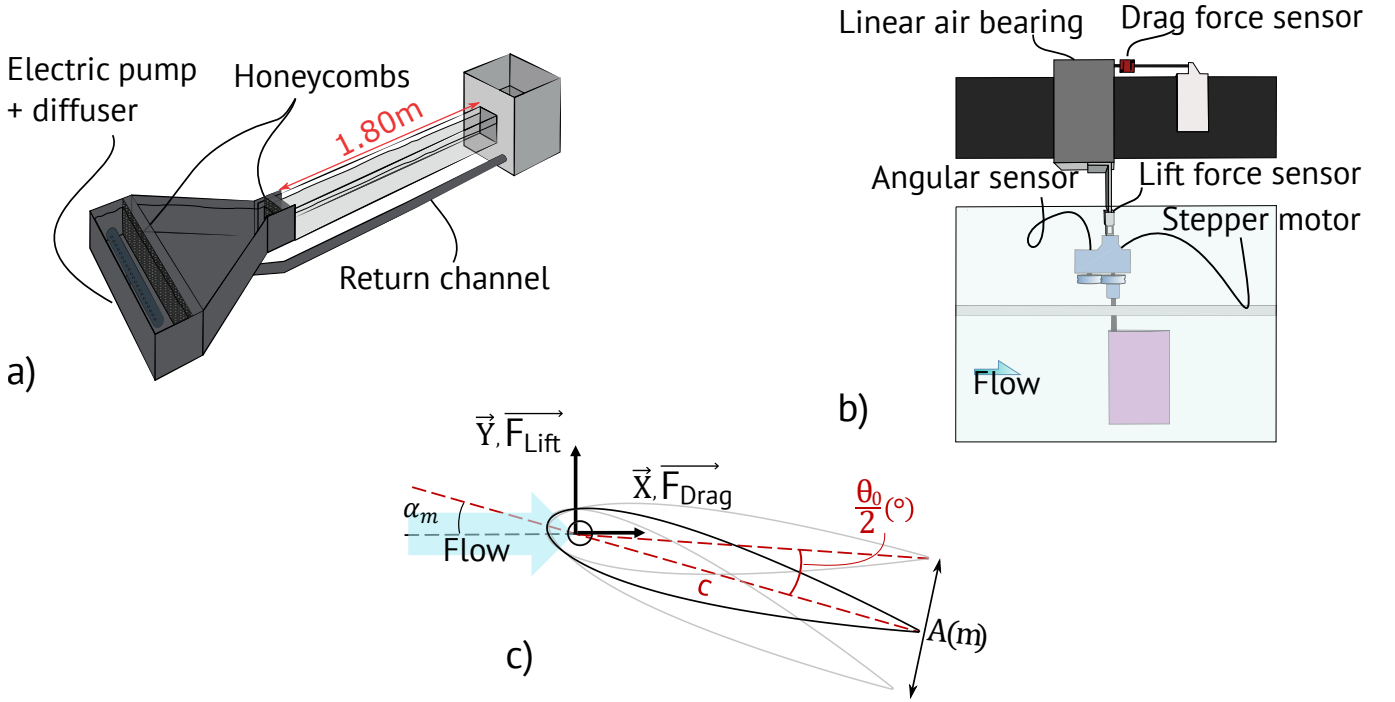


FIG. 2: a) Closed loop water channel with a length of 1.80 m and a cross-section with water of $0.2 \times 0.2 \text{ m}^2$ [30]. b) Acquisition setup to measure forces and kinematics data. c) Sketch in top-view of an experiment. The trailing edge is always more than 5.5 cm from the wall. This value is reached in the extreme case where $\alpha_m = 28^\circ$ and $\theta_0 = 11^\circ$.

II. EXPERIMENTAL SETUP AND METHODS

Experiments were performed in a free surface water channel in a closed loop with a 0.2 m by 0.2 m section. Thanks to the several honeycombs upstream of the test area, the turbulence intensity measured by Particle Image Velocimetry is below 5% (Figure 2.a).

The experiments are performed with a foil NACA 0018 3D printed in PLA with a chord $c = 0.08 \text{ m}$, a span $s = 0.12 \text{ m}$ which gives an aspect ratio $AR = 1.5$. The rotation axis for the pitching movement is located at $0.1c$ from the leading edge. The axis is a carbon rod attached to a stepper motor that also drives an angular position sensor. The ensemble rotation motor + foil is mounted on a load sensor (CLZ639HD) which measures the lift component (Y) of the force. This system previously presented is in a sliding connection with an air cushion in relation to the frame (Figure 2.b). A second load sensor (FUTEK LSB210) working in traction and compression, located between the linear air bearing and the frame, records the drag force. We sample analogically all the physical parameters and we control the command sent to the stepper motor with a National Instruments card (NI-USB-6221) which allows us to record data at a frequency of 1024 Hz.

The pitching motion is characterized by the angle between the flow direction and the chord of the foil as $\theta(t) = \alpha_m + (\theta_0/2) \sin(2\pi ft)$, where α_m is the mean angle of incidence. The angular position sensor allows controlling the mean incidence angle (α_m) between the foil and the flow, like in a real case with the incidence of the sail and the airflow. The amplitude swept by the trailing edge is $A/2 = c \sin(\theta_0/2)$ (Table I).

The following experiments were performed at a flow velocity $U_\infty = 0.18 \text{ m/s}$ corresponding to a Reynolds number based on the chord $Re = 14400$, (Table I). By controlling the frequency, amplitude and mean angle of incidence of the sinusoidal motion of the foil, and thanks to the two force sensors, we are able to study unsteady propulsion as a function of the physical and kinematic parameters of the pitching motion described in the Table I.

| Reynolds number, $Re = \frac{\rho U_\infty c}{\mu}$ | Mean incidence angle, $\alpha_m(^{\circ})$ | Reduced frequency, $k = \frac{\pi f c}{U_\infty}$ | Amplitude of pitching, $A/2 = c \sin(\frac{\theta_0}{2}) \text{ (m)}$ | Strouhal number, $St_A = \frac{Af}{U_\infty}$ |
|--|---|--|--|--|
| 14400 | [-8, 30]] | [2.45, 4.20] | [0.0027, 0.0162] | [0.045, 0.27] |

TABLE I: Physical parameters describing our experiments.

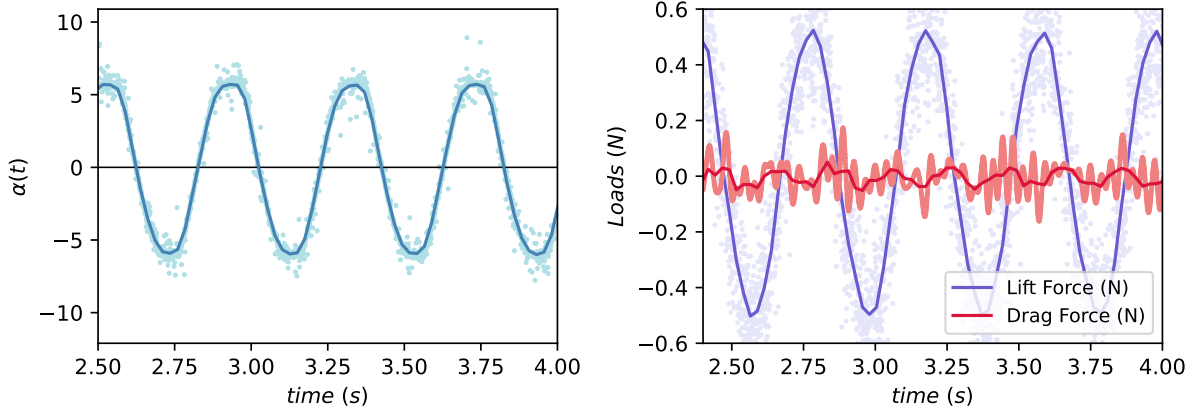


FIG. 3: Raw (points) and filtered (lines) data of incidence angle (left) and unsteady forces (right) versus time, for an experiment where $\alpha_m = 0^\circ$, $\theta_0 = 12^\circ$ and $f = 2$ Hz ($St_A = 0.2$). We have smoothed here over 0.1 s with a Savitsky-Golay filter of order 1.

We studied the hydrodynamic forces for different values of α_m in the range of $[-8, 30]$, of St_A in the range $[0.045, 0.27]$ and f in the range of $[1.75, 3]$ Hz with an increment of 1° , 0.045 and 0.25 Hz respectively (Table 1). For each α_m , measurements are made by selecting our St_A range and the frequency range. As we are testing six frequencies, there will be six experiments per St_A value. An amplitude A is coupled to each frequency value tested in order to achieve the desired St_A value. Finally, we measure the mean value of lift and drag for the couple (St_A, α_m) . We run experiments for each case during 30 cycles, and we extract the mean value of forces.

We define the aerodynamic coefficients as :

$$C_D = \frac{\overline{F_{\text{Drag}}}}{\frac{1}{2}\rho S U_\infty^2} \quad \text{and} \quad C_L = \frac{\overline{F_{\text{Lift}}}}{\frac{1}{2}\rho S U_\infty^2} \quad (1)$$

C_L and C_D represent the lift and the drag coefficient, where ρ is the fluid density (1000 kg/m^3), $S = s \times c$ is the lifting surface (0.0096 m^2), U_∞ is the flow velocity (0.18 m/s) and F_{Drag} and F_{Lift} the drag and the lift force, respectively. Due to the size of the water tank, a correction for the blockage effect is taken into account. For our experimental set-up the blockage area ratio S_a/S_{tank} is between 4% and 9%, where S_{tank} is the cross flow surface of the water tank ($S_{\text{tank}} = 0.04 \text{ m}^2$) and S_a is the projected surface orthogonal to the flow of the foil depending on the mean incidence angle. We use in (2) a correction with a quasi-streamlined flow method for three-dimensional bluff-body changing its mean incidence angle according to the ESDU Technical Committees [31].

$$\frac{C_{*,c}}{C_*} = 1 - \lambda_1 \lambda_3 \lambda_5 \left(1 + \frac{1}{\lambda_2} \frac{s}{c} \right) \frac{c S_a}{S_{\text{tank}}^{1.5}} - 0.5 C_D \frac{S_a}{S_{\text{tank}}} \quad (2)$$

$C_{*,c}$ represents the force coefficient corrected and C_* the raw coefficient. Where, $\lambda_1 = 0.72 \times (l/h + h/l)$ is the water tank shape parameter for a three-dimensional flow. l and h are respectively the width and the height of the water tank. $\lambda_2 \approx 0.83$ is the body shape parameter. $\lambda_3 \approx \lambda_{3, \text{ellipsoid}} \times 0.25 + \lambda_{3, \text{cone}} \times 0.75$ is the body volume parameters. $\lambda_5 = 1 + 1.1 \times (c/w) \times (\pi/180)^2 \times \alpha_m^2$, for taking into account the projected width when α_m in degree changes. w is the maximum width of the foil.

III. RESULTS AND DISCUSSION

A. The aerodynamic coefficients on the foil

Figure 4 presents the lift and drag coefficients as a function of the mean incidence angle for all cases tested. The kinematics is represented by the Strouhal number in the third dimension (colorbar). The force coefficients for the static behaviour of the foil are represented by the open circle symbols. The static stall appears at $\alpha_m = 16^\circ$, where $\partial C_L / \partial \alpha_m$ is equal to 0.07 a bit lower than $\pi^2/90$, the theoretical result given by the two-dimensional thin airfoil theory (blue line) [32]. This is due to the 3D effect caused in particular by the small aspect ratio of the foil used. The collapse of the experimental results for different reduced frequencies

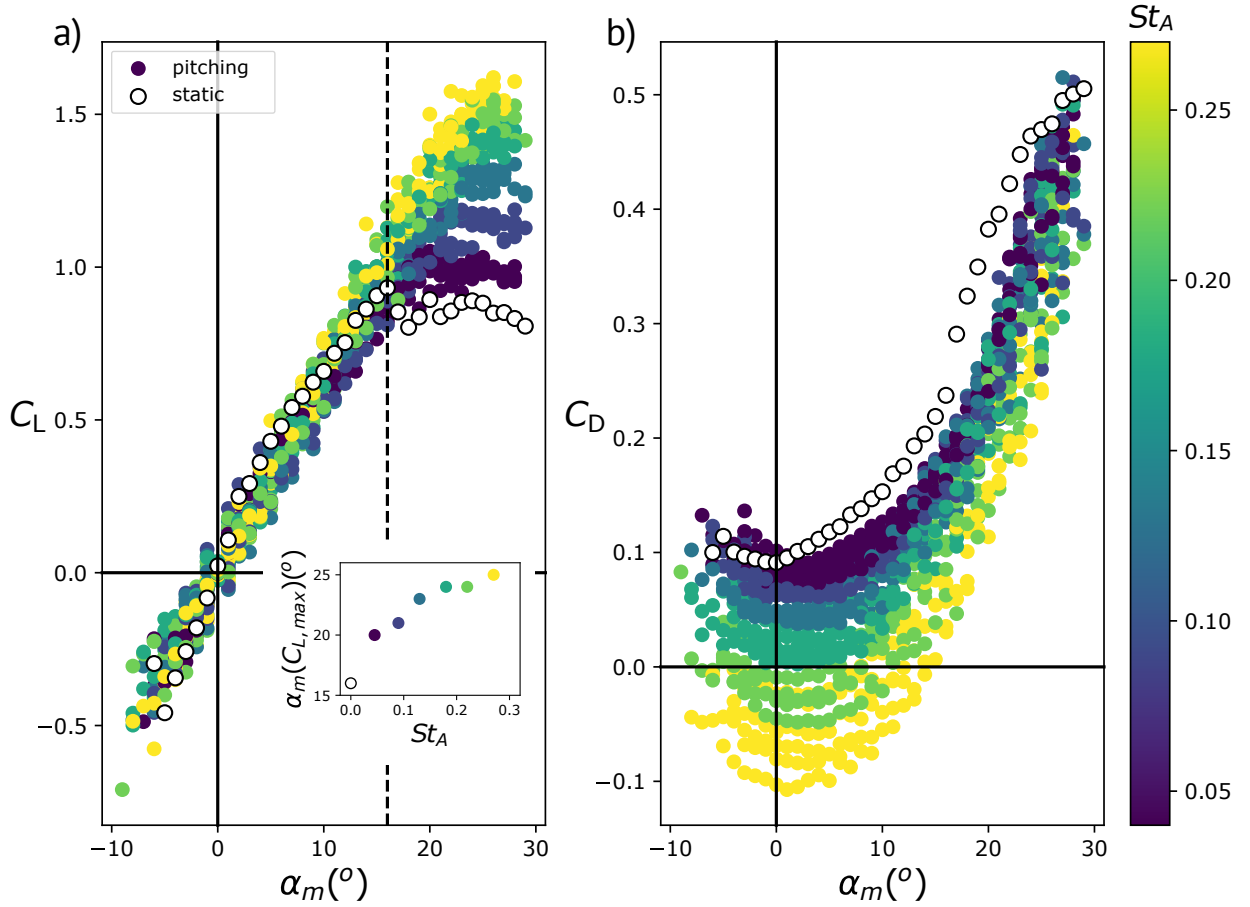


FIG. 4: Lift and drag coefficients as a function of the mean incidence angle for a range of Strouhal numbers. a) Lift coefficients. The vertical dashed line crosses $\alpha_m = 16^\circ$ where the static stall appears. In insert, we show the value of α_m where the maximum of lift coefficient is reached as a function of St_A . b) Drag coefficients.

but the same Strouhal number (in particular for the lift coefficient) shows that the Strouhal number St_A , is the most appropriate parameter to describe the effect of pitching on the forces generated, rather than the reduced frequency.

The lift coefficient C_L increases linearly for all the range of St_A up to the static stall angle. As illustrated in the inset of Figure 4.a, an increase in St_A is accompanied by a corresponding rise in the mean incidence associated with maximum lift. The range where a linear relationship between C_L and α_m holds is wide, and the directing slope increases as a function of St_A . Even oscillations with the smallest St_A tested increase the lift produced while delaying the onset of the threshold. It is worth noting that the first notable effect of the dynamic pitching of the foil is to delay the stall point with respect to α_m . The first and most important consequence of this effect is to maintain the growth of C_L beyond the stall transition of the static case. This effect is even more pronounced as St_A increases to reach a maximum pitching lift coefficient $(C_L)_{pitching, max} \approx 1.6$ (compared to ≈ 1 for the static case). Cleaver et al. [33, 34] studied the behaviour of the lift force generated by a plunging foil with a non-zero incidence angle. The static stall angle for this foil is 10° . For an incidence angle equal to 12.5° and 15° , they showed a threshold in St_A where C_L does not increase anymore and fatally falls. It appears that at an angle of incidence of 20° , this drop in C_L as a function of St_A no longer occurs. In the case of plunging, there is therefore a limit to the generation of lift in certain cases.

Figure 4.b shows that for all experiments carried out and for $\alpha_m > 0^\circ$, the drag generated when pitching is lower than the static value. More importantly, a drag-thrust transition can be observed: the more we increase St_A , the more the drag is reduced, until a critical value of Strouhal number $St_A = 0.18$, where drag becomes negative, meaning that the foil generates thrust. At high enough $St_A \approx 0.27$ and for a specific couple of frequency and beating amplitude, the pitching motion generates thrust in a range of $\alpha_m [-8^\circ; +15^\circ]$. In the case of a pitching foil with a zero mean incidence angle, maximum propulsive efficiency is reached for $St_A \approx 0.3$ [23]. In addition, the physiological limits of the athletes will limit the range of St_A potentially usable by the athletes.

Previous works in the literature have examined the dynamics of oscillating foils at large incidences [24, 25]. Seshadri et al. [35] conducted numerical investigations of the flow for the same system of Ohmi et al. [24, 25], focusing on one mean incidence angle equal to 30° , a beating amplitude equal to $\pm 15^\circ$, and two reduced frequencies $k = 0.628, 3.14$. They demonstrated that as the reduced frequency increases, a LEV is maintained for a longer duration, resulting in a significant enhancement of lift. The

amplitudes tested in our study are lower than those observed in the aforementioned studies. Due to blockage in the channel, the amplitude, denoted by $\theta_0/2$, is constrained to a value of at most 11° . This leads to a maximum incidence angle of 39° at a given instant. It would be interesting to ascertain whether the dynamics remain unchanged when the same St_A is considered with larger amplitudes.

Summarizing, Figure 4.a shows that, as St_A increases, lift also increases, with the growth being more significant at higher mean incidence angles. This behaviour is observed for all incidence angles, including those beyond the static stall angle. The pitching motion is thus effective in delaying stall. Additionally, as shown in Figure 4.b, increasing St_A leads to a decrease in drag, regardless of the amount by which St_A is increased.

B. Generation of propulsion forces in a context of sailing system

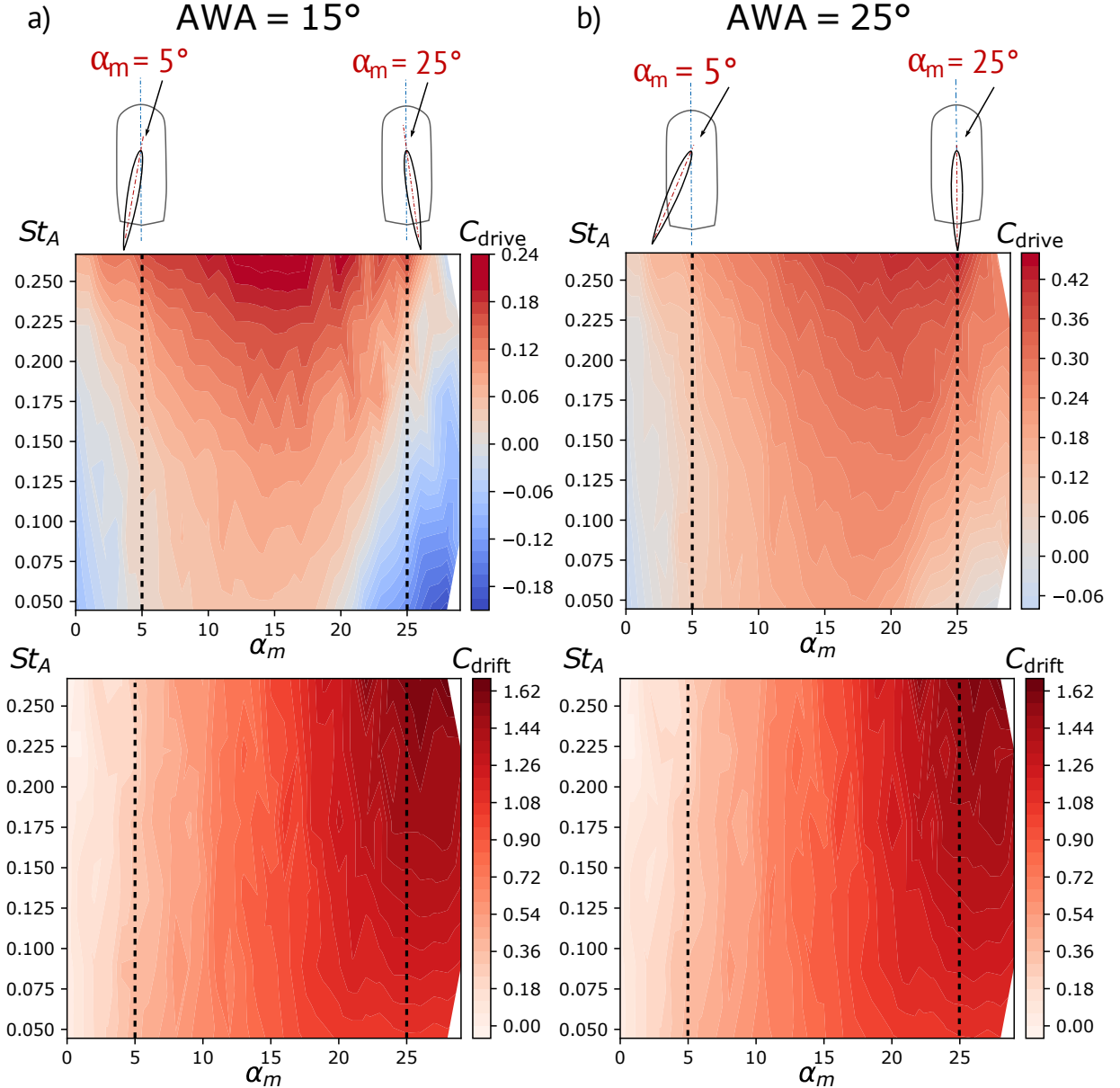


FIG. 5: Mapping of the sailing coefficients C_{drive} and C_{drift} as a function of pitching parameter St_A and mean incidence angles α_m . The coefficients are averaged by group of St_A . In upwind conditions for windsurf, AWA is mostly included between 15° (a) and 25° (b). Note that for C_{drive} (a, b), the colorbars do not indicate the same range of coefficients.

To put the previous results into the context of sailing, we project the force generated by the sail in the frame of the boat (see

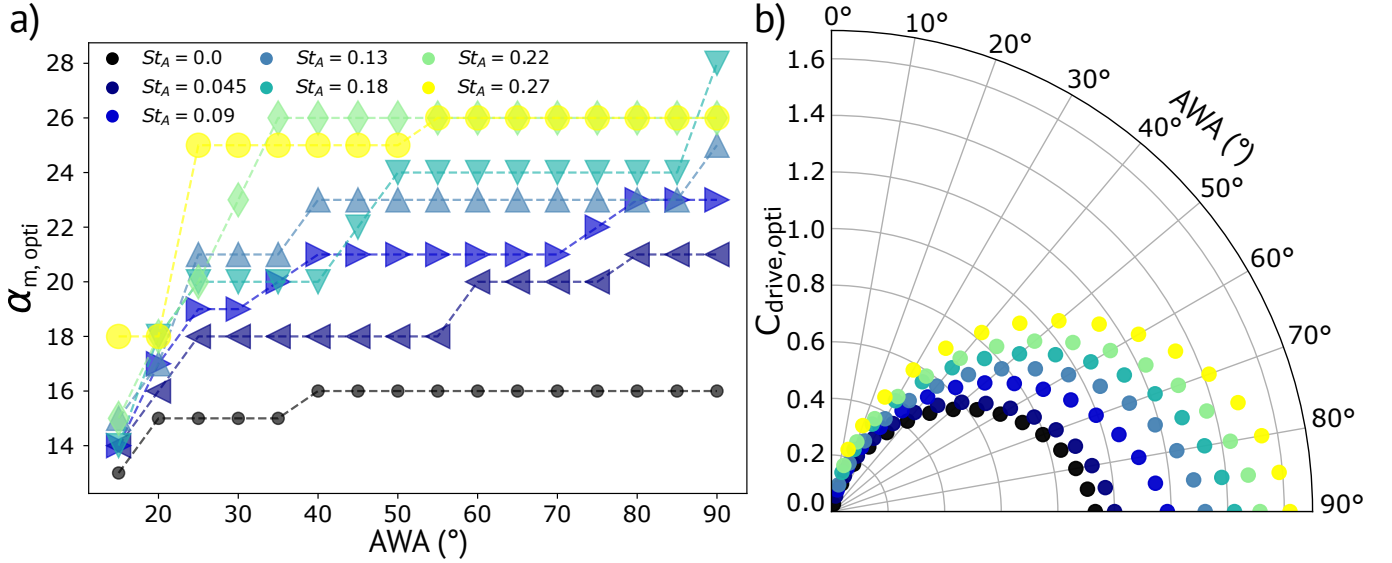


FIG. 6: a) $\alpha_{m, opti}$ as a function of AWA. b) Polar of the optimum drive coefficient $C_{drive, opti}$ as a function of AWA. They are represented for each value of St_A experimentally studied. For each AWA we only plot the optimal value, and we determine for each St_A the mean incidence angle $\alpha_{m, opti}$ according to $C_{drive, opti}$.

Figure 1), defining a drive force and a drift force. These can be written in terms of their respective force coefficients C_{drive} and C_{drift} as:

$$C_{drive} = C_L(\alpha_m) \sin(AWA) - C_D(\alpha_m) \cos(AWA), \quad (3)$$

$$C_{drift} = C_L(\alpha_m) \cos(AWA) + C_D(\alpha_m) \sin(AWA), \quad (4)$$

where AWA is the Apparent Wind Angle (Figure 1.b). AWA and α_m are completely independent, but it is clear that some positions of the sail or the foil according to the direction of the boat are not realistic [12]. Figure 5 shows the effective sailing coefficients as a function of the mean incidence angle α_m and St_A for two values of AWA 15° and 25° upwind sailing, which are classical positions in windsurfing. The values presented on the maps are averaged according to the Strouhal number for different values of f and A .

In both cases (AWA 15° and 25°), Figure 5 (bottom row) shows that for $\alpha_m \lesssim 20^\circ$ C_{drift} is more sensitive to an increase of the mean incidence angle than to an increase of the Strouhal number. For $\alpha_m \gtrsim 20^\circ$, C_{drift} depends mainly on St_A . With the goal of maximizing the sailing speed and reducing the racing time, both C_{drive} and C_{drift} need to be optimised. These will be the tools to manage the boat's course, depending on the race strategy. For the two studied AWA values representing the boundaries of the typical upwind navigation range, the C_{drift} values are almost identical. This is due to the fact that $C_L \cos(AWA) \gg C_d \sin(AWA)$ because $\sin(AWA) < \cos(AWA)$ and $\cos(AWA) \approx 1$. Figure 5.a shows that pitching generates drive force coefficient with a maximum $C_{drive, max} \approx 0.24$. When AWA is 15°, it becomes evident that as St_A increases, the range of α_m capable of generating propulsion ($C_{drive} > 0$) expands. For instance, at $St_A = 0.05$, the propulsion range is $5^\circ \leq \alpha_m \leq 20^\circ$ with the lowest values of C_{drive} reached compared with those reached for the other Strouhal numbers of the study. At $St_A = 0.25$, the range broadens to $0^\circ \leq \alpha_m \leq 25^\circ$. As AWA increases, the range of α_m where $C_{drive} > 0$ increases too, as can be seen in Figure 5, comparing the top row of .a (AWA = 15°) and .b (25°). Non-efficient zones where the propulsion generated by pumping is less than or close to zero ($C_{drive} \leq 0$) are located at low α_m close to zero and at the largest angles studied here. The negative zone for the largest angles comes from the influence of the term $C_D(\alpha_m) \cos(AWA)$ in Equation 3. For AWA = 15° in the low α_m range (top left panel), the increase of the driving force with St_A is very visible and corresponds to the drag to thrust transition mentioned on Figure 4. Moving from AWA = 15° to AWA = 25°, the term $C_D(\alpha_m) \cos(AWA)$ decreases, and it becomes easier to generate drive force.

To optimise the travelled speed, we want to maximise the C_{drive} coefficient. From the working map (St_A, α_m) of C_{drive} , we now determine the optimal drive coefficient $C_{drive, opti}$ for each value of St_A and the mean incidence angle $\alpha_{m, opti}$ associated with this optimal value, which are illustrated in Figure 6. For each value of St_A , the experimental data shows that $\alpha_{m, opti}$ increases as a function of AWA. In Figure 6.b, the driving force is always larger when pitching compared to the static case (black, $St_A = 0$).

Let us look at the case where $C_{drive} \approx 0.6$ in Figure 6.b. Increasing St_A will make it possible to maintain the value of $C_{drive, opti}$ while reducing AWA, in this case potentially going from AWA = 55° in static to AWA = 35° if the oscillation rises to a St_A of 0.3.

This corresponds to a variation in the angle of incidence, $\alpha_{m, opti}$, between 16° and 25° . Using unsteady propulsion, the boat can maintain its forward momentum while sailing upwind more efficiently. Reducing the AWA reduces the distance travelled and potentially reduces the number of tack changes needed. Tacking implies in most cases that the board is not lifted anymore, so reducing the distance travelled and potentially the number of tack changes can definitely reduce the race time.

Another race strategy can be highlighted using Figure 6.a. Athletes may want to maintain their trajectory and therefore maintain AWA constant while increasing $C_{drive, opti}$. Let's take the case where they want to keep an $AWA = 25^\circ$. The athletes will then have to modify the mean incidence angle according to how they increase the St_A associated with an increase in C_{drive} . This strategy will then result in a threefold increase of the driving force coefficient from 0.18 up to at most 0.44 for as long as the pumping motion is maintained.

In this section, we have discussed how to generate the most beneficial pitching possible, as well as various navigation strategies that can optimize the trajectory and propulsion of the craft. We now need to compare unsteady and steady propulsion.

We present in Figure 7.a and .c the sailing force polars as a function of the mean incidence angle for $AWA = 20^\circ$, which is a classical position of upwind in windfoil. These polars summarise the behaviour of the driving and drifting forces. In order to compare the effect of pitching propulsion with that of stationary propulsion, we introduce a parameter that quantifies the impact of pitching compared with standard propulsion, defined as:

$$\delta C_* = \frac{C_{*,pitch} - C_{*,static}}{|C_{*,static}|}. \quad (5)$$

We plot the sailing force polars of the impact coefficients of drive δC_{drive} and of drift δC_{drift} in Figure 7.b and .d. The data for δC_{drive} and δC_{drift} for $\alpha_m = 3^\circ$ is not shown because the static value for $C_{drive, static}$ is very close to zero and so the impact coefficient is very large.

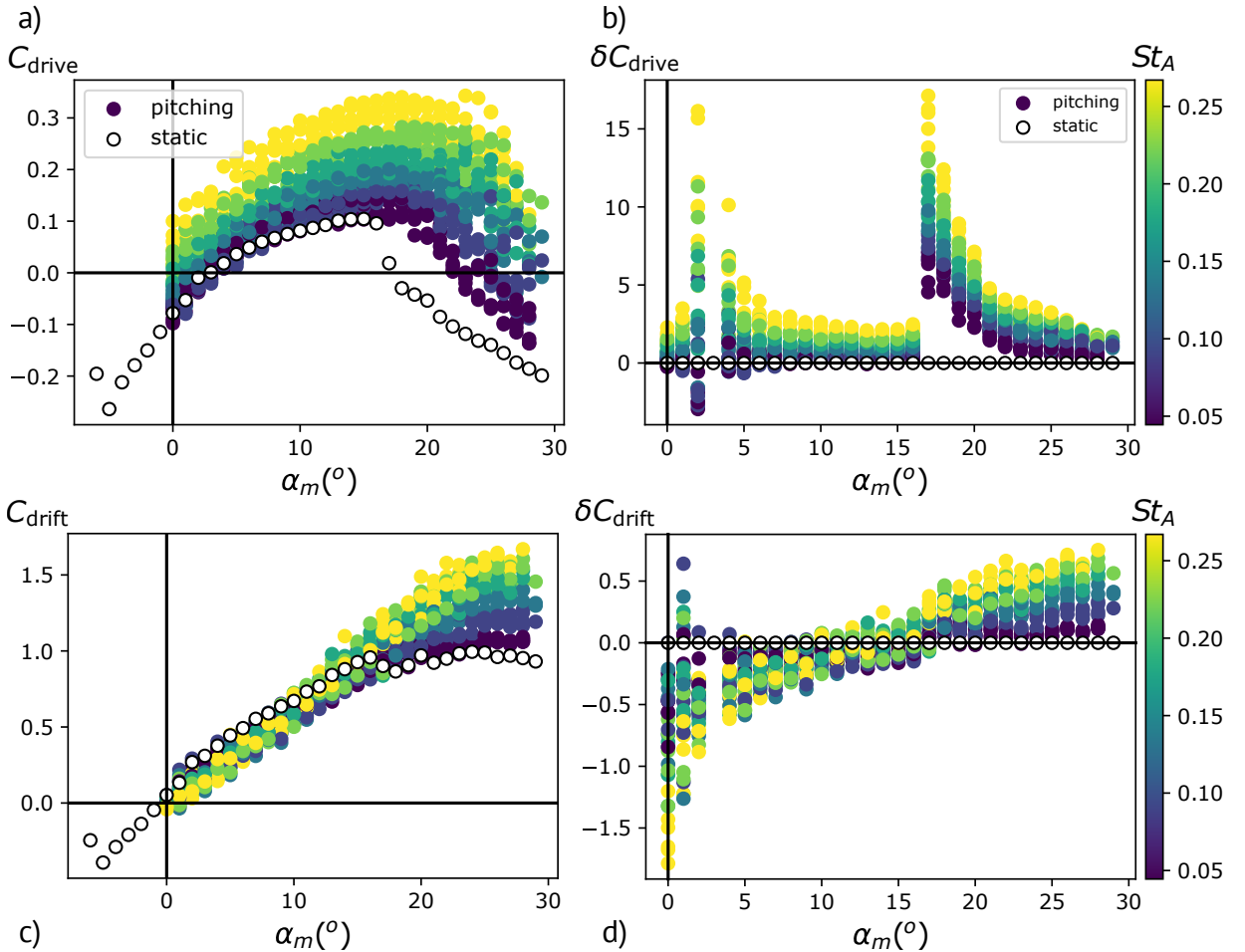


FIG. 7: Sailing force polars of drive and drift coefficients and impact coefficient polars as a function of the mean incidence angle for $AWA = 20^\circ$. a) C_{drive} , b) δC_{drive} , c) C_{drift} d) δC_{drift} .

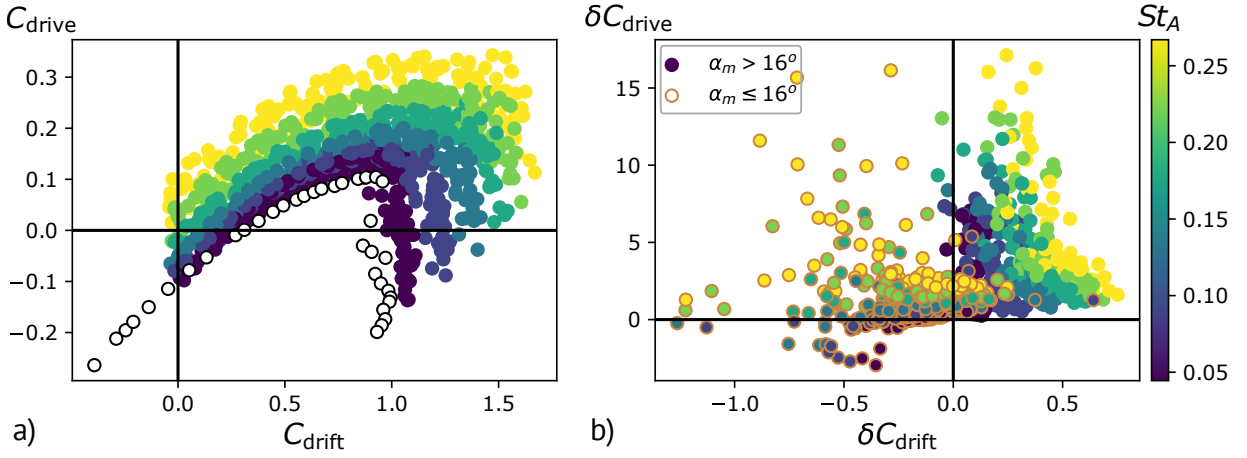


FIG. 8: Operating polars for AWA = 20°. a) C_{drive} vs C_{drift} . b) δC_{drive} vs δC_{drift} .

In Figure 7.a, the static polar of C_{drive} reveals a stall occurring at $\alpha_m = 16^\circ$, beyond which no propulsion is generated ($C_{\text{drive}} \leq 0$). When athletes employ pumping techniques, they notably enhance the drive force compared to the static condition, with particularly significant improvements at mean incidence angles exceeding 16° . In the lowest range of α_m some pitching cases seem to be ineffective compared to the steady propulsion. With the use of the impact coefficient, Figure 7.b highlights these ineffective cases. We can see for $\alpha_m \leq 8^\circ$ some impact coefficients are negative. It shows an inefficiency to pitch for these cases, for example at $\alpha_m = 2^\circ$ (Figure 7.c) where $St_A = 0.045$ or $St_A = 0.09$. For $8^\circ < \alpha_m \leq 16^\circ$, δC_{drive} depends weakly on α_m but depends on St_A . Figure 7.d shows the sailing polar of δC_{drift} as a function of α_m . δC_{drift} increases linearly and becomes positive for all St_a at $\alpha_m = 18^\circ$. Below this value of mean incidence angle, using unsteady propulsion reduces the drift coefficient.

Finally, we discuss this impact coefficient applied to the drive and drift forces at AWA = 20° in Figure 8. Figure 8.a shows the operating polar of C_{drive} versus C_{drift} , while that of δC_{drive} as a function of δC_{drift} is shown in Figure 8.b, summarizing the impact of pitching on propulsion. We separate the values into two parts: those for $\alpha_m \leq 16^\circ$ (circled in orange) and those for $\alpha_m > 16^\circ$.

In Figure 8.b, for $\alpha_m \leq 16^\circ$ few values of δC_{drive} are negative and so in these cases pumping the foil is detrimental. However, within this range of α_m and during pitching, for most of the studied cases, it is possible to reduce the drift force generated by the steady propulsion of the sail—a capability applicable in most scenarios. During a race, sail pumping can thus enable athletes to maintain their course more effectively by reducing C_{drift} without compromising the propulsive force C_{drive} , ultimately resulting in shorter race times. In the second part at higher α_m , a distinct behaviour emerges with respect to St_A , where increasing St_A maximizes δC_{drive} .

IV. CONCLUSION

We experimentally investigated the dynamic response of a foil oscillating about its vertical axis, examining how the mean angle of incidence impacts transient forces. Within the studied physical parameter ranges (Table I), we discovered the potential to generate lift coefficients nearly double the static values at mean angles of incidence exceeding the static stall angle, with a pronounced dependence on St_A . Moreover, pitching the foil delays the stall angle and increases C_L past the static stall value. Up to the static stall angle, the increase in C_L is not primarily governed by St_A . However, for low α_m ranges, we observed a classical result where C_D depends on St_A and exhibits a drag-propulsion transition. The relationship is not singularly determined by frequency, amplitude, or Strouhal number, but rather by their combined interaction, as highlighted by Floryan et al. [23]. Drawing an analogy with sailing, particularly windsurfing, we introduced coefficients C_{drive} , C_{drift} to characterize the forces applied in the boat's frame. We found that C_{drift} depends on α_m rather than St_A , while C_{drive} demonstrates an increasingly expansive operating range ($C_{\text{drive}} > 0$) that grows with St_A . From these observations, we determined the maximal propulsive force and its associated optimal mean incidence angle ($\alpha_{m, \text{opti}}$) for upwind conditions (AWA < 90°). Critically, studying drive force in conjunction with drift force becomes essential for racing strategic considerations. The potential scenarios include either changing position by increasing the drift force or increasing speed without altering course by focusing solely on forward force. The final segment of our study presents the coefficient differences between pitching and static conditions, highlighting the

performance gains achieved through unsteady propulsion.

-
- [1] K. Mok, P. Zhou, J. Hou, S. Zhong, X. Zhang, R. C.-H. So, and K. Chan, Performance of a windsurfing sail under steady condition, *Ocean Engineering* **289**, 10.1016/j.oceaneng.2023.116295 (2023).
- [2] I. Viola and R. Flay, Force and pressure investigation of modern asymmetric spinnakers, *Transactions of the Royal Institution of Naval Architects Part B: International Journal of Small Craft Technology* **151**, 31 (2009).
- [3] F. Fossati, S. Muggiasca, and I. Viola, Wind tunnel techniques for investigation and optimization of sailing yachts aerodynamics, in *2nd High Performance Yacht Design Conference* (2006) pp. 105–113.
- [4] I. Viola and R. Flay, Full-scale pressure measurements on a sparkman and stephens 24-foot sailing yacht, *Journal of Wind Engineering and Industrial Aerodynamics* **98**, 800 (2010).
- [5] I. Viola and R. Flay, Sail pressures from full-scale, wind-tunnel and numerical investigations, *Ocean Engineering* **38**, 1733 (2011).
- [6] F. Fossati, I. Bayati, S. Muggiasca, A. Vandone, G. Campanardi, T. Burch, and M. Malandra, Pressure measurements on yacht sails: Development of a new system for wind tunnel and full scale testing, in *SNAME Chesapeake Sailing Yacht Symposium* (SNAME, 2016) p. D011S001R007.
- [7] J. Banks, A. Webb, T. Spenkuch, and S. Turnock, Measurement of dynamic forces experienced by an asymmetric yacht during a gybe, for use within sail simulation software, *Procedia Engineering* **2**, 2511 (2010).
- [8] F. Fossati and S. Muggiasca, Experimental investigation of sail aerodynamic behavior in dynamic conditions, *Journal of Sailboat Technology* **2**, 1 (2011).
- [9] B. Augier, P. Bot, F. Hauville, and M. Durand, Experimental validation of unsteady models for fluid structure interaction: Application to yacht sails and rigs, *Journal of Wind Engineering and Industrial Aerodynamics* **101**, 53 (2012).
- [10] B. Augier, P. Bot, F. Hauville, and M. Durand, Dynamic behaviour of a flexible yacht sail plan, *Ocean Engineering* **66**, 32 (2013).
- [11] N. Aubin, B. Augier, P. Bot, F. Hauville, M. Sacher, and R. Flay, Wind tunnel investigation of dynamic trimming on upwind sail aerodynamics, *Journal of Sailing Technology* , 111 (2016).
- [12] J. D. Young, S. E. Morris, R. R. Schutt, and C. H. K. Williamson, Effect of hybrid-heave motions on the propulsive performance of an oscillating airfoil, *J. Fluids Struct.* **89**, 203 (2019).
- [13] P. Zhou, S. Zhong, H. Jiang, X. Zhang, and R. C.-H. So, Propulsive efficiency and efficacy of a pumping sail, *Physics of Fluids* **33**, 10.1063/5.0065561 (2021).
- [14] J. Eldredge, J. Toomey, and A. Medina, On the roles of chord-wise flexibility in a flapping wing with hovering kinematics, *Journal of Fluid Mechanics* **659**, 94 (2010).
- [15] W. McCroskey and J. William, Unsteady airfoils, *Annual Review of Fluid Mechanics* 10.1146/annurev.fl.14.010182.001441 (1982).
- [16] M. Triantafyllou, G. Triantafyllou, and D. Yue, Hydrodynamics of fishlike swimming, *Annual Review of Fluid Mechanics* **32** (2000).
- [17] J. Izraelevitz and M. Triantafyllou, Adding in-line motion and model-based optimization offers exceptional force control authority in flapping foils, *Journal of Fluid Mechanics* **742**, 5 (2014).
- [18] M. Platzer, K. Jones, J. Young, and J. Lai, Flapping-wing aerodynamics: Progress and challenges, *AIAA Journal* **46**, 2136 (2008).
- [19] M. Koochesfahani, Vortical patterns in the wake of an oscillating airfoil, *AIAA journal* **27**, 1200 (1989).
- [20] J. M. Anderson, K. Streitlen, D. S. Barrett, and M. S. Triantafyllou, Oscillating foils of high propulsive efficiency, *J. Fluid Mech.* **360**, 41 (1998).
- [21] Q. Zhong and D. B. Quinn, Predicting the slowly converging dynamics of asymmetric vortex wakes, *Physical Review Fluids* **9**, 064702 (2024).
- [22] R. Godoy-Diana, J.-L. Aider, and J. Wesfreid, Transitions in the wake of a flapping foil, *Physical Review E* **77**, 016308 (2008).
- [23] D. Floryan, T. Van Buren, C. W. Rowley, and A. J. Smits, Scaling the propulsive performance of heaving and pitching foils, *J. Fluid Mech.* **822**, 386 (2017).
- [24] K. Ohmi, M. Coutanceau, T. Loc, and A. Dulieu, Vortex formation around an oscillating and translating airfoil at large incidences, *Journal of Fluid Mechanics* **211**, 37 (1990).
- [25] K. Ohmi, M. Coutanceau, O. Daube, and T. Loc, Further experiments on vortex formation around an oscillating and translating airfoil at large incidences, *J. Fluid Mech.* **225**, 607 (1991).
- [26] L. Schouveiler, F. Hover, and M. Triantafyllou, Performance of flapping foil propulsion, *Journal of fluids and structures* **20**, 949 (2005).
- [27] N. Chiereghin, D. Cleaver, and I. Gursul, Unsteady lift and moment of a periodically plunging airfoil, *AIAA Journal* **57**, 208 (2019).
- [28] X. Zheng, S. Pröbsting, H. Wang, and Y. Li, Characteristics of vortex shedding from a sinusoidally pitching hydrofoil at high Reynolds number, *Phys. Rev. Fluids* 10.1103/PhysRevFluids.6.084702 (2021).
- [29] A. Mackowski and C. Williamson, Direct measurement of thrust and efficiency of an airfoil undergoing pure pitching, *J. Fluid Mech.* **765**, 524 (2015).
- [30] T. Aurégan, B. Thiria, and S. Courrech du Pont, Scaling the thrust and deformations of a rotor with flexible blades, *Physical Review Fluids* **8**, 044401 (2023).
- [31] R. Gilbey and P. Chappell, Lift-interference and blockage corrections for two-dimensional subsonic flow in ventilated and closed wind-tunnels, Technical Report, ESDU 76028, The Royal Aeronautical Society (1995).
- [32] L. Milne-Thomson, *Theoretical aerodynamics* (Dover Publications, 1973) Chap. 7.13, p. 117.
- [33] D. Cleaver, Z. Wang, and I. Gursul, Lift enhancement on oscillating airfoils, in *39th AIAA fluid dynamics conference* (2009) p. 4028.
- [34] D. J. Cleaver, Z. Wang, and I. Gursul, Bifurcating flows of plunging aerofoils at high strouhal numbers, *Journal of Fluid Mechanics* **708**, 349 (2012).

- [35] P. Seshadri, A. Aravind, and A. De, Leading edge vortex dynamics in airfoils: Effect of pitching motion at large amplitudes, [Journal of Fluids and Structures](#) **116**, 103796 (2023).